Hydroxyapatite-Supported Ruthenium Catalysts in Ammonia Synthesis: Impact of Ba and Cs as Catalyst Promoters

Héctor Uriel Rodríguez Vera, Christophe Coquelet, Thomas Deleau, Armando Izquierdo Colorado, Olivier Bouchard, Doan Pham Minh

Hydroxyapatite-Supported Ruthenium Catalysts in Ammonia Synthesis: Impact of Ba and Cs as Catalyst Promoters

Héctor Uriel Rodríguez Vera, Christophe Coquelet, Thomas Deleau, Armando Izquierdo Colorado, Olivier Bouchard, and Doan Pham Minh*

This work is devoted to the synthesis, the characterization, and the evaluation of hydroxyapatite-supported ruthenium catalysts, with or without Ba and/or Cs promotion. Thus, a series of catalysts containing Ru, Cs, and Ba was synthesized by the incipient wetness impregnation method. Such catalysts are characterized by different physicochemical methods, providing insights into their properties. These catalysts are evaluated in the ammonia synthesis reaction at 350–500 °C and 10–25 bar. Sample 1Ru/hydroxiapatite (HAP), without promoter, shows a negligible catalytic activity, due to the formation of large Ru nanoparticles, which are not favorable for the formation of ammonia. On the other hand, the addition of Cs and Ba improves the catalytic performance, and Ba is found to be better than Cs. The pretreatment of the barium-containing catalysts under Ar flow at 600 °C is also found to be crucial for the decomposition of barium nitrate into barium oxide, thereby enhancing catalytic activity.

1. Introduction

Ammonia (NH_3) is a chemical compound with various important applications, particularly in the production of fertilizers.[1] To date, at the industrial scale, ammonia is mostly produced by the well-known Haber–Bosch process, where nitrogen reacts with hydrogen at high temperatures (450–500 °C) and high pressures (ca. 150 bar) over promoted iron catalysts.[2] These harsh operating conditions make the Haber–Bosch process energy-intensive (35×10^3 MJ per ton of produced NH_3, accounting for up to 2% of the global annual energy production).[2] Moreover, ammonia production has a high environmental carbon footprint. Solely the reaction generates up to 750 kg of CO_{2eq} per ton of NH_3 produced, raising to 2.4 ton of CO_{2eq} per ton of NH_3 if the environmental impact of H_2 production is included; thus, accounting for ca. 2.5% of global greenhouse gas emissions.[3] More recently, ammonia has become a promising alternative renewable energy carrier, allowing efficient storage of hydrogen produced by water electrolysis using renewable electricity.[4,5] Indeed, ammonia can be liquefied under softer conditions in comparison to the necessary conditions for hydrogen liquefaction, therefore, facilitating its storage and its transportation.[6] Note that the critical temperature of H_2 is 33.1 K, whereas NH_3 critical temperature is 405.6 K and, consequently, their boiling temperatures are 20.4 K and 233.8 K, respectively. Moreover, NH_3 can also be directly used as an alternative fuel in combustion engines[7] or in electricity generation by direct combustion in gas turbines.[8] Thus, optimizing energy efficiency and accounting for the environmental impact of ammonia industrial production play an important role in the context of the current ecological transition.

Current commercially available catalysts are predominantly promoted Fe-based catalysts. Examples of commercial iron-based catalysts are the historic BASF catalysts, such as the *S6-10* (**Table 1**), in which iron oxides are doped with different promoters. Alumina and calcium oxide are used to increase the specific surface area and to protect the active phase (α-Fe_2O_3 crystals) from thermal sintering.[9] Potassium oxide and magnesium oxide are used to promote the structural stability of the catalyst and, more specifically, to enhance its catalytic activity. Their presence increases the adsorption heat of molecular nitrogen of nearby iron superficial atoms, hence lowering the activation energy barrier for the dissociation of nitrogen.[10,11] Other commercial catalysts employing Ru as the active phase are also available, one such example is the *KT Al_2O_3 Ru Type K-04502* catalyst from Heraeus, which contains 2 wt% Ru dispersed on the surface of an alumina support.[12]

Effort has been devoted to the quest for an efficient ammonia synthesis catalyst that softens the industrial operation conditions of the reaction.[3,13,14] As recently reviewed by Humphreys et al.[14] various approaches have already been explored in order to maximize ammonia production rate: control of support morphology; use of promoters; use of various kinds of nitrides, hydrides, oxyhydride nitrides, electrides, etc., as the active phases. Generally, among the various active metals, ruthenium is among the most

Table 1. Atomic composition (wt%) of the commercial catalyst BASF S6−10 used for ammonia production.[9,11]

Bulk composition (atomic %)					
	Fe	K	Al	Ca	O
Fresh catalyst	40.5	0.35	2.0	1.7	53.2
Superficial composition (atomic %)[a)]					
Unreduced catalyst	8.6	36.1	10.7	4.7	400
Reduced catalyst[b)]	11.0	27.0	17.0	4.0	41.0

[a)]by Auger electron spectroscopic analysis; [b)]analysis performed after the sample has been exposed to normal atmospheric conditions.

active phases, only after osmium.[1] B-5 sites, as previously described,[15] have been identified as likely the most active sites in ammonia synthesis (and also ammonia decomposition). They are mostly present on small Ru nanoparticles of ca. 1.8–2.5 nm. Moreover, the catalytic performance of Ru-based catalysts can be improved by promoters, such as Ba, K, Cs, Li, etc.[16–20] More specifically, Cs can improve the activity of Ru catalysts by forming hot ring promotion zones around Ru crystals,[18] while BaO may have an electron-donor effect, and $BaCO_3$ may act as a high melting compound, preventing the aggregation of small Ru particles.[21] About the catalyst supports studied for the dispersion of Ru nanoparticles, carbonaceous materials seem to be the most intensively investigated. This is attributed to their low cost and interesting physicochemical properties, such as high specific surface area and a broad spectrum of possible structural morphologies, which typically result in a high initial catalytic activity.[17,21–31] For example, the catalyst 3.4 wt%Ru–3.4 wt% Ba/CNT displayed a specific ammonia production rate of 110 000 $\mu mol_{NH3}\ g_{cat}^{-1}\ h^{-1}$ at 450 °C, 100 bar.[32] However, under the typical operation temperatures of the ammonia synthesis, carbon supports can react with hydrogen, that is, catalyzed by Ru nanoparticles, causing catalyst deactivation and surface loss. The treatment of these supports with promoters such as Na, Cs, Ba, La, etc., may improve the performance of carbon-supported ruthenium catalysts.[17,26,27,29,33,34] Various metal oxides, such as MgO, CeO_2, ZrO_2, Al_2O_3, La_2O_3, Pr_2O_3, etc., with or without the presence of promoters, have also been largely investigated as supports of Ru catalysts.[14,35] Lanthanides seemed to be the most efficient supports by comparing the specific ammonia production rate: 60 200 $\mu mol_{NH3}\ g_{cat}^{-1}\ h^{-1}$ over 5wt%Ru/$La_{0.5}Pr_{0.5}O_{1.75}$ at 400 °C, 10 bar and a WHSV of 72 L $g_{cat}^{-1}\ h^{-1}$, or 64 000 $\mu mol_{NH3}\ g_{cat}^{-1}\ h^{-1}$ over 5 wt%Ru/Pr_2O_3 at 400 °C, 10 bar and a WHSV of 72 L $g_{cat}^{-1}\ h^{-1}$[14]. However, lanthanide availability is limited and may present competition with other applications.

In recent decades, hydroxyapatite ($Ca_{10}(PO_4)_6(OH)_2$, called thereafter hydroxiapatite (HAP) has garnered growing attention in its use as a catalyst material.[36] This is due to its physicochemical properties such as the possibility of showing a high specific surface area, good thermal stability, tailorable acidity/basicity, as well as good ion exchange capacities,[36] HAP has been studied as catalysts or catalyst supports in different chemical processes, such as reforming of methane and other hydrocarbons, selective oxidation of alcohols and alkanes, selective hydrogenation and dehydrogenation of hydrocarbons, organic synthesis, etc.[36]. However, to-date and according to our knowledge, there are still very few studies on HAP-based catalysts in ammonia synthesis. Only a preprint (submission under review) was found at the moment of the writing of this article, wherein Ru/HAP catalysts containing 2–4 wt%Ru showed the specific ammonia production rate of 49–329 $\mu mol_{NH3}\ g_{cat}^{-1}\ h^{-1}$ at 300–400 °C and 1 bar.[37] This result seems to be very promising since the studied catalysts show good performance at 1 bar.

The present work is devoted to the investigation of HAP-supported Ru catalysts, with and without the addition of Ba and Cs as catalyst promoters. The objective is to design a performing catalyst that can work under mild conditions of temperature (up to 500 °C) and pressure (up to 25 bar).

2. Results and Discussion

As mentioned in the experimental section, $Ba(NO_3)_2$ is not easy to decompose under air,[38] while $CsNO_3$ may decompose and/or volatilize above 700 °C.[39] Thus, the thermal behavior of Ba- and Cs-containing catalysts was investigated under air (**Figure 1**a,c) and under Ar (Figure 1b,d). Before the thermogravimetric analysis (TGA), both the precursors of Ba and Cs were only dried at 105 °C after their deposition on Ru/HAP.

Under the air flow (Figure 1a,c), the HAP support shows a consecutive mass loss within the investigated temperature range, which is characteristic of this material.[40,41] This mass loss could be due to the elimination of free water and carbonate species adsorbed or inserted in the apatitic structure of HAP. The HAP-based catalysts show thermogravimetry (TG) profiles, which are more or less similar to that of the HAP support. No further distinct mass loss due to the decomposition of residual metal precursors could be observed up to 700 °C under the air atmosphere, as highlighted by the differential thermogravimetry (DTG) curves in Figure 1c.

Under Ar, the thermal behavior of these materials is different (Figure 1b,d). All four materials show an initial mass gain at the beginning of the TGA analysis (DTG peaks below 100 °C). Two materials containing $CsNO_3$ show a second broad mass gain within ca. 100–300 °C, which needs further investigation for understanding. Above 300 °C, HAP and 1Ru2Cs/HAP do not display significant DTG peaks,while 1Ru2Ba/HAP and 1Ru1Cs1Ba/HAP (both containing $Ba(NO_3)_2$) displayed net DTG peaks, suggesting a possible decomposition of barium nitrate under Ar.[38] For this reason, two Ba-containing catalysts pretreated under Ar (1Ru2Ba/HAP_Ar and 1Ru1Cs1Ba/HAP_Ar) were investigated in the ammonia synthesis reaction, in order to evidence the impact of this thermal pretreatment on their catalytic performance (see the catalyst list in **Table 2**).

Figure 2a shows the Fourier transform infrared (FTIR) spectra of the HAP support and the 1Ru/HAP catalyst calcined under air at 300 °C. Characteristic peaks of phosphate groups in the apatitic structure of the HAP support can be observed within the wavelength ranges of 650–500 cm^{-1} and 1200–900 cm^{-1}.[42,43] Some trace amounts of carbonate groups and nitrate groups were still

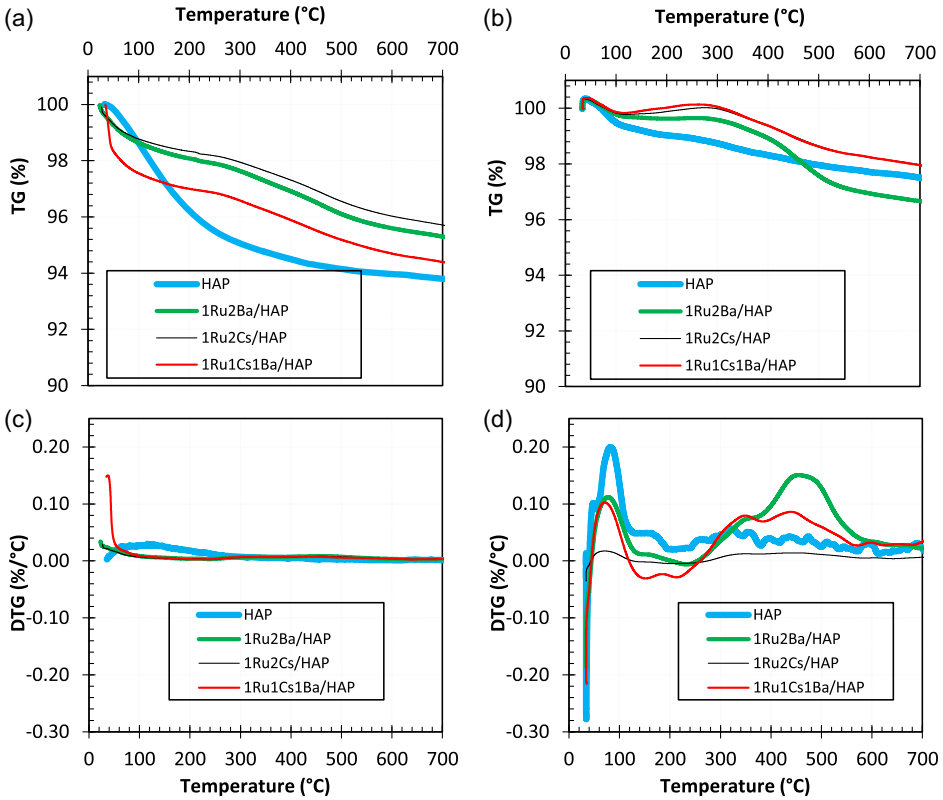

Figure 1. TGA of the HAP support and the prepared catalysts: a) TGA curves under air flow; b) TGA curves under argon flow; c) DTG curves under air flow; and d) DTG curves under Ar flow.

Table 2. List of catalysts prepared in this work and their specific surface area (BET surface).

Catalyst	Targeted metal loading [wt%]	BET surface [$m^2\ g^{-1}$]
HAP	0	75
1Ru/HAP	Ru: 1	60
1Ru2Ba/HAP	Ru: 1	53
	Ba: 2	
1Ru2Cs/HAP	Ru: 1	52
	Cs: 2	
1Ru1Cs1Ba/HAP	Ru: 1	51
	Cs: 1	
	Ba: 1	
1Ru2Ba/HAP_Ar	Ru: 1	40
	Ba: 2	
1Ru1Cs1Ba/HAP_Ar	Ru: 1	51
	Cs: 1	
	Ba: 1	

present on the surface of the Ru/HAP catalyst. The presence of carbonate groups and nitrate groups could be confirmed by analysis of carbon, hydrogen, nitrogen and sulfur (CHNS) analysis (Figure 2b) for the HAP support for other catalysts. The presence of carbonate groups can be explained by their possible incorporation into the apatitic structure during the contact of the HAP support and the Ru/HAP catalyst with the air. The smoothness around the OH^- band at around 3500 cm^{-1} indicates that the trapped water is almost nonexistent. These observations were similar for the other catalysts (results not shown). By CHNS analysis (Figure 2b), nitrogen was well present in the Ba- and Cs-containing catalysts, since these analyses were done with the dried materials, while hydrogen was present in the form of free water and hydroxyl groups in the HAP structure.

Figure 3a–e shows the nitrogen adsorption/desorption isotherms of the support and the dried catalysts, while Figure 3f,g shows the nitrogen adsorption/desorption isotherms of 1Ru2Ba/HAP_Ar and 1Ru1Cs1Ba/HAP_Ar. In all cases, the form of these isotherms is similar for all the materials studied. According to the IUPAC classification,[44] isotherms of type V, which are characteristic of mesoporous materials, are observed. All the materials show likely a H2 type hysteresis. From these isotherms, the Barret–Joyner–Halenda (BJH) model could be applied to determine the distribution of pore volume of the materials. In comparison with the initial HAP support, the deposition of the active phases seemed to limit the fraction of small mesopores (Figure 3h).

X-ray diffraction (XRD) patterns of the HAP support, 1Ru/HAP catalyst (calcined under air flow at 300 °C), and Ba- and Cs-containing catalysts, which were dried or pretreated under flowing Ar at 600 °C, are displayed in **Figure 4** (more details on XRD results are available in Figure S1, Supporting Information). In comparison with the initial HAP support, the deposition of the active phases did not affect the crystalline

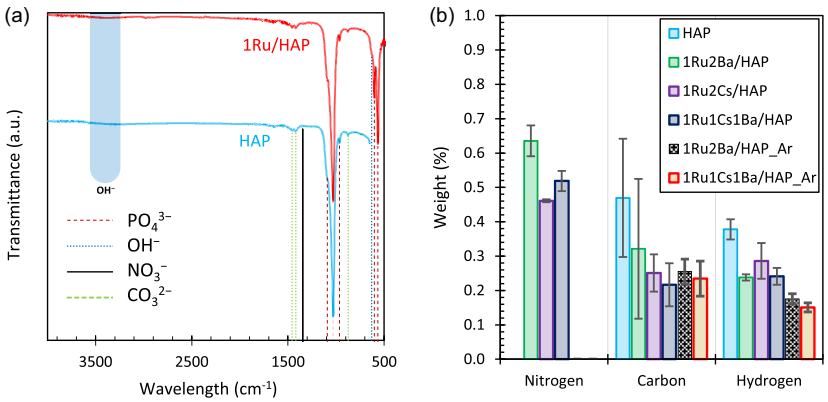

Figure 2. FTIR spectra a,b) CHNS results of the HAP support and Ru-based catalysts.

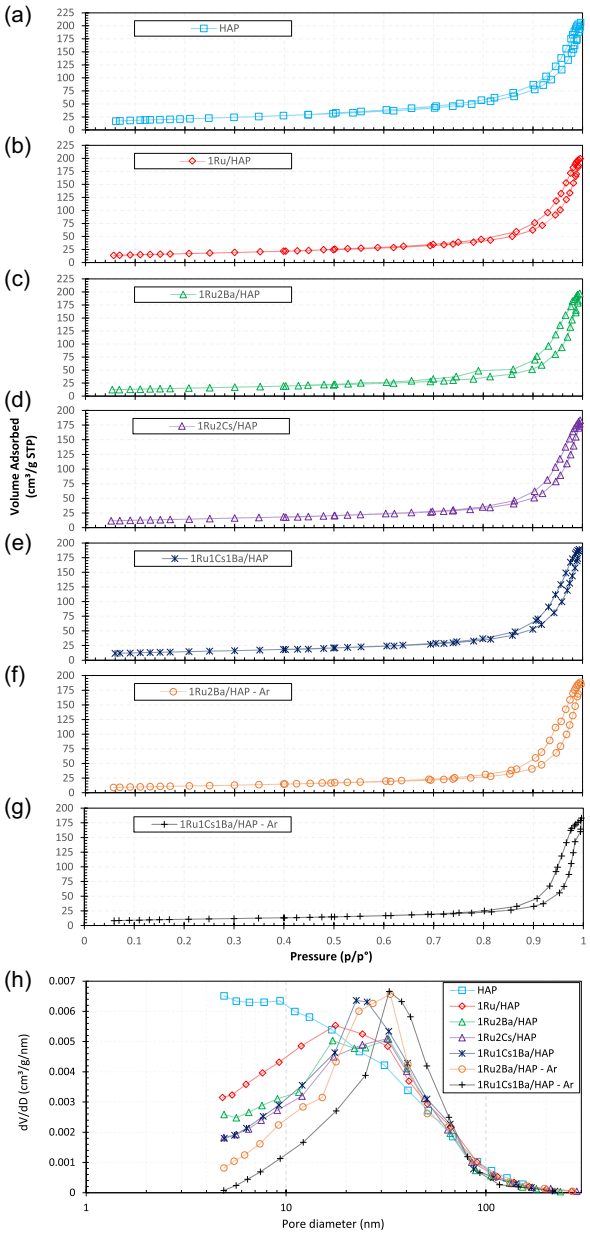

Figure 3. a–g) Nitrogen adsorption/desorption isotherms, and h) BJH pore volume distributions of the HAP support and Ru-based catalysts.

phases of the support, since all the diffraction peaks of the support were found again in all the prepared catalysts. As expected, the presence of RuO_2 (main peaks at 28.019°, 35.066°, and 54.267°) is confirmed for all the prepared catalysts investigated. The first peak of RuO_2 at 28.019° is superposed but shows higher intensity in comparison with the peak of the HAP support. The second and the third peaks of RuO_2 at 35.066° and 54.267°, which are practically far from the peaks of the HAP support, are well visible in the prepared catalysts that confirms the formation of RuO_2 (see also Figure S1a, Supporting Information). For the dried Cs-containing catalysts (1Ru2Cs/HAP and 1Ru1Cs1Ba/HAP), the presence of $CsNO_3$ is confirmed by the peak corresponding to the plane (111) at 19.86° (see also Figure S1b, Supporting Information). No diffraction peak belonging to Cs_2O was observed in these dried Cs-containing catalysts (see also Figure S1d, Supporting Information). For the dried Ba-containing catalysts (1Ru2Ba/HAP and 1Ru1Cs1Ba/HAP), the diffraction peaks of $Ba(NO_3)_2$, which correspond to the planes (111), (131), and (222) at 18.919°, 36.686°, and 38.88°, are well-visible (see also Figure S1c, Supporting Information). On the other hand, the diffraction peaks of $Ba(NO_3)_2$ are no more visible in the Ba-containing catalysts pretreated under Ar flow at 600 °C (1Ru2Ba/HAP_Ar and 1Ru1Cs1Ba/HAP_Ar (see also Figure S1c, Supporting Information). Thus, the thermal decomposition of $Ba(NO_3)_2$ was successfully achieved, and it is believed to have most probably led to the formation of BaO. However, the main diffraction peaks of BaO overlap with the peaks of HAP; therefore, its presence cannot be satisfactorily confirmed through XRD (see also Figure S1e, Supporting Information).

Figure 5 presents scanning electron microscopy (SEM) images of the HAP support and the catalysts, which were dried under air or pretreated under Ar at 600 °C. In general, no significant change was observed for the HAP surface after the deposition of the active phases, except for the addition of these new phases. In Figure 5b1,b2, the 1Ru/HAP catalyst, calcined at 300 °C under air flow, clearly shows the formation of large RuO_2 nanoparticles (size up to dozens nm as indicated by green arrows). These particles are relatively large in comparison with those reported in the literature for other catalyst supports.[45–48] The dried multimetallic catalysts, 1Ru2Cs/HAP (Figure 5c1–c3), 1Ru2Ba/HAP (Figure 5d1–d3), and 1Ru1Cs1Ba/HAP (Figure 5e1–e3), show similarly shaped

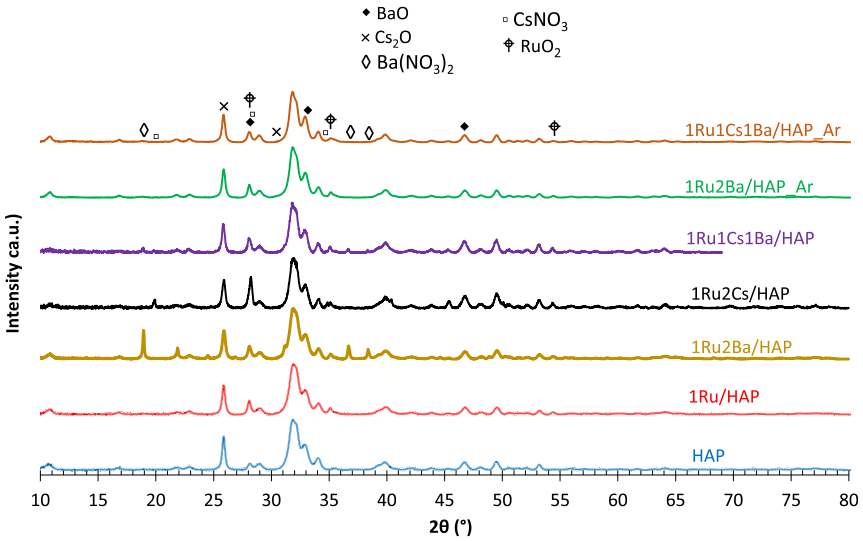

Figure 4. XRD patterns of the HAP support and the Ru-based catalysts.

RuO_2 nanoparticles (green arrows) in comparison with the 1Ru/HAP catalyst. Large agglomerates of $Ba(NO_3)_2$ and $CsNO_3$ (red arrows) are also observed and confirmed by energy-dispersive X-ray spectroscopy (EDX) analysis (results not shown). In the case of the catalysts pretreated under Ar flow, the observations are different. On sample 1Ru2Ba/HAP_Ar (Figure 5f1), the shape of RuO_2 nanoparticles (green arrow) is similar to those in the dried catalysts, but BaO particles of much larger sizes are also observed (yellow arrows). Similarly, for 1Ru1Cs1Ba/HAP_Ar (Figure 5g1,g2), RuO_2 nanoparticles are still present; however, it was not possible to observe Ba- or Cs-based particles. Several punctual spot EDX analyses were performed, but these elements (Ba and Cs) were not detected. Nonetheless, a long EDX analysis on a large zone of the catalyst surface demonstrated Ba and Cs to be present in amounts close to the theoretical values (see Table S1, Supporting Information). Thus, the hypothesis is that, for the catalyst 1Ru1Cs1Ba/HAP_Ar, Ba and Cs existed under a very dispersed form due to the Ar pretreatment, i.e., their incorporation into the apatitic structure of the HAP support, rendering them invisible to SEM.

TEM images and metal particle size distribution of the catalysts, which were calcined under air flow at 300 °C ((a1), (a2)), dried under air ((b1), (b2), (c1), (c2), (d1), (d2)), or pretreated under Ar flow at 600 °C ((e1), (e2), (f1), (f2)) are displayed in **Figure 6**. On 1Ru/HAP catalyst (Figure 6a1,a2), the largest RuO_2 nanoparticles were observed up to ca. 110 nm. This confirms SEM results observed in Figure 5b1,b2. In the case of the multimetallic catalysts, it was not possible to distinguish Ba and Cs nanoparticles. Therefore, the particle size distribution curves only describe particles majorly or entirely composed of RuO_2. For the dried catalysts, because the Ba and Cs precursors were not decomposed, the particle size distribution curves describe only RuO_2 nanoparticles. Indeed, these dried catalysts had roughly similar mean particle diameters when compared with that of the monometallic catalyst. For the catalyst 1Ru2Ba/HAP_Ar (Figure 6e1e2), despite the fact that large BaO particles exist, as evidenced by SEM analysis (Figure 5f1), the mean particle diameter was estimated (19.5 nm) to be smaller than that of the monometallic catalyst (22.1 nm). Finally, the catalyst 1Ru1Cs1Ba/HAP_Ar had a smaller mean particle diameter (16.7 nm) in comparison with that of the monometallic catalyst (22.1 nm). The hypothesis is that the Ar pretreatment influenced, although in a limited fashion, on promoting the dispersion of all the metal particles. Further characterization will be needed to better understand the effect of thermal treatment under Ar on RuO_2 nanoparticle size.

Figure 7a displays the temperature programmed reduction (TPR) profiles of the different materials. The HAP support has no significant TPR signal within 30–900 °C. The 1Ru/HAP catalyst shows multimodal peaks within 140–320 °C, which correspond to the reduction of Ru species. These temperatures are found to be slightly smaller than those reported in the literature,[47,48] which might be due to large RuO_2 nanoparticles in the 1Ru/HAP catalyst, being easier to be reduced. All three multimetallic catalysts without Ar treatment (i.e., 1Ru2Ba/HAP, 1Ru2Cs/HAP, and 1Ru1Cs1Ba/HAP) also show multimodal TPR peaks within 140–320 °C. However, the peaks around 240–320 °C are much larger than those of the monometallic catalyst (1Ru/HAP), suggesting that the reduction of Cs(II) and Ba(II) species should also take place. Two catalysts pretreated under Ar (i.e., 1Ru2Ba/HAP_Ar and 1Ru1Cs1Ba/HAP_Ar) show two reduction peaks: the first multimodal peak at around 200 °C, which might be attributed to the reduction of Ru species, and the second large and weak peak at around 680 °C, which might be due to Ba and Cs species incorporated in the apatitic structure. In all cases, TPR profiles justify the choice of the in situ reduction temperature of 350 °C before doing catalytic tests, since this reduction temperature allows reducing most of Ru, Ba, and Cs species. The CO_2-temperature programmed desorption (TPD) profiles in Figure 7b show only very weak desorption peaks, meaning that all the investigated materials should contain a low density of basic sites. On the other

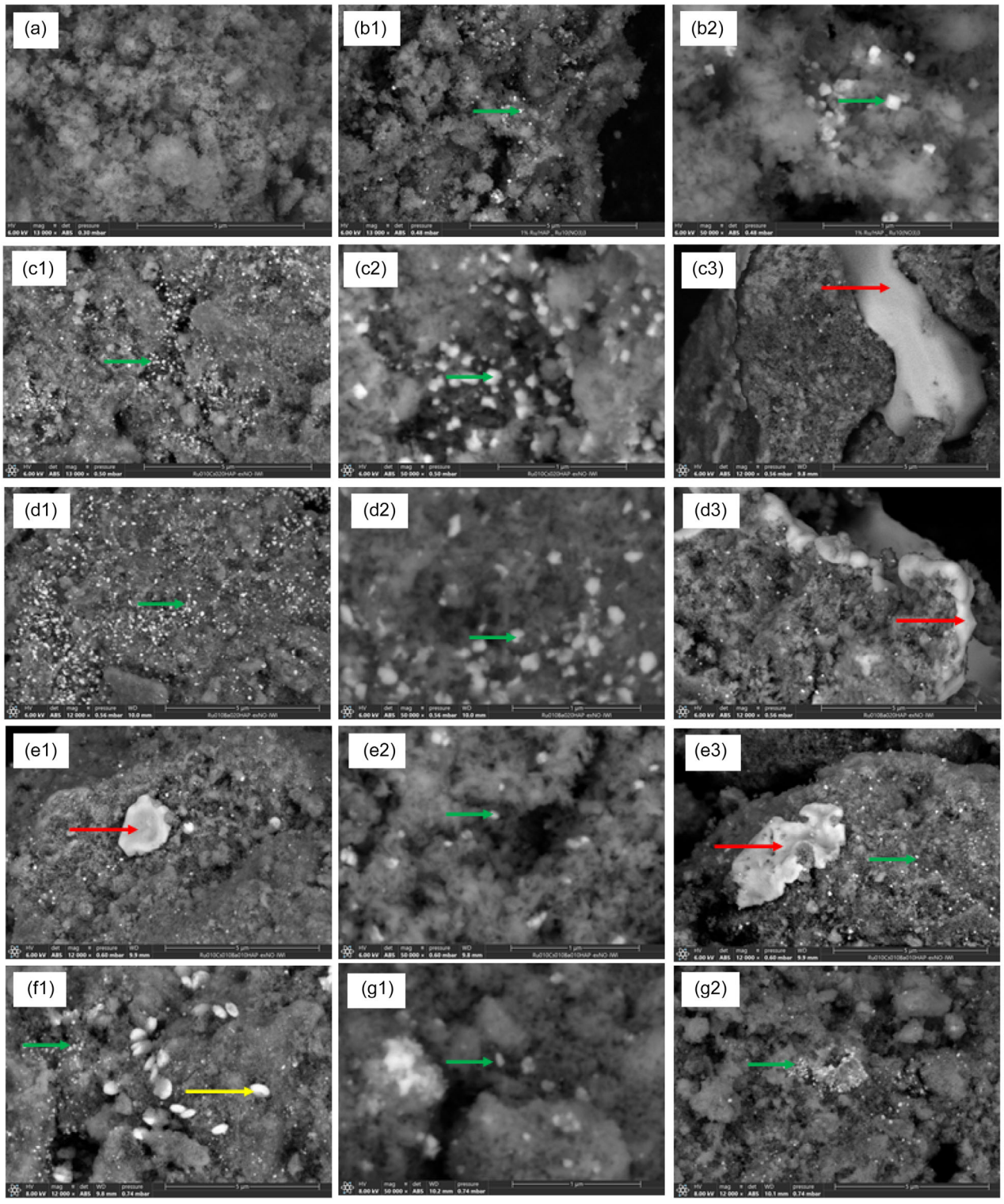

Figure 5. a) SEM images of HAP support; b1,b2) 1Ru/HAP; c1–c3) 1Ru2Cs/HAP; d1–d3) 1Ru2Ba/HAP; e1–e3) 1Ru1Cs1Ba/HAP; f1) 1Ru2Ba/HAP_Ar; and g1,g2) 1Ru1Cs1Ba/HAP_Ar. The images were obtained at a magnification of 12,000× (c3,d1,d3,e1,e3, f1,g2); 13,000× (a,c1,b1); and 50,000× (b2,c2,d2,e2,g2).

hand, NH_3-TPD in Figure 7c displays two large desorption peaks centered at around 150 and 420 °C, suggesting the presence of at least two types of acidic sites. However, the second peak centered at around 420 °C is much weaker for 1Ru2Ba/HAP_Ar and 1Ru1Cs1Ba/HAP_Ar, suggesting a lower density of acidic sites in these materials, in comparison with other materials.

Table 3 shows the catalytic performance of the catalysts in ammonia synthesis. The HAP support did not present any

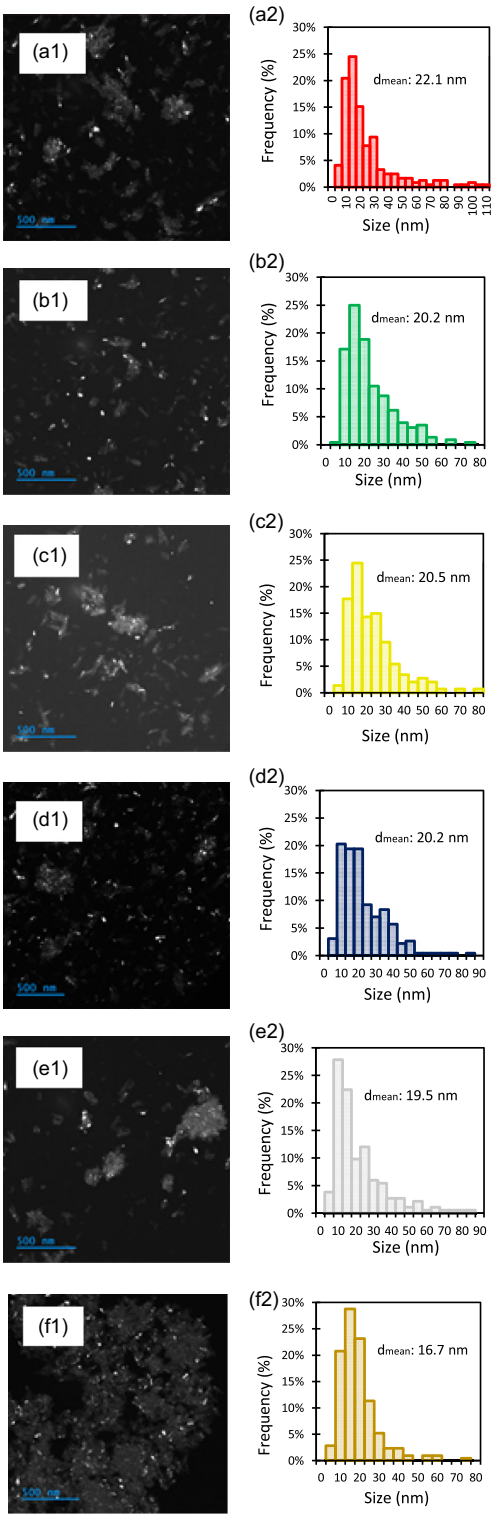

Figure 6. TEM images and particle size distribution of: a1,a2) 1Ru/HAP; b1,b2) 1Ru2Ba/HAP; c1,c2) 1Ru2Cs/HAP; d1,d2) 1Ru1Cs1Ba/HAP; e1,e2) 1Ru2Ba/HAP_Ar; and f1,f2) 1Ru1Cs1Ba/HAP. All these TEM images were obtained at a magnification of 15,000×.

measurable activity under all the conditions of temperature and pressure investigated. The monometallic catalyst, 1Ru/HAP (#1), had only very low catalytic activity around 450–500 °C and 25 bar.

The addition of Cs (#3, 1Ru2Cs/HAP) improved the catalytic activity of the monometallic catalyst, which shows the formation of ammonia even at 350 °C and 10 bar (the 1st reaction step). By keeping the pressure unchanged at 10 bar, the average ammonia production rate progressively increased as the reaction temperature increased from 350 to 400 and 450 °C (the 2nd and the 3rd reaction steps). However, increasing the total reaction pressure to 25 bar led to a decrease in the average ammonia production rate. Consequently, turnover frequency (TOF) values also followed the same trend. This may be due to the following raisons: i) the catalyst might suffer from deactivation; and/or ii) the increase of the pressure favors the adsorption of basic molecules of NH_3 on the surface of acidic alumina support, which was used in each test to keep the catalyst bed at the center of the reactor tube (see section 2.4). The first reason could be confirmed by Figure S2, Supporting Information, where progressive loss of the catalytic activity is shown at each condition of temperature and pressure (green and red arrows showing the decrease of the ammonia production rate). The first preliminary results of SEM analysis of used catalysts suggested that sintering phenomena might take place during the reaction (Figure S3, Supporting Information), but this would be further confirmed by other characterizations, such as high resolution transmission electron microscopy (HR-TEM). For the second reason, it has been reported in the literature that ammonia could be effectively adsorbed on activated alumina.[49] To confirm the NH_3 adsorption by the sintered alumina powder used in the present work, an NH_3-TPD analysis was performed with this material. Figure S4, Supporting Information, shows a small desorption peak centered at ca. 150 °C that confirms the adsorption of NH_3 on this support. Also, it can be observed in Figure S2, Supporting Information, that the deactivation is more pronounced at 450 °C and 25 bar (red arrow) than those at 340–450 °C and 10 bar (green arrows), and when the total pressure is already at 25 bar, the deactivation is less pronounced (500 °C and 25 bar by the blue arrow against 450 °C and 25 bar by the red arrow).

The addition of the second promoter (#2 in Table 3, 1Ru1Cs1Ba/HAP) improved the catalytic activity of the bimetallic 1Ru2Cs/HAP catalyst (#3 in Table 3). Thus, Ba seems to be better than Cs as a promoter for Ru/HAP catalysts. Thus, by doping the monometallic catalyst with only Ba (#4 in Table 3, 1Ru2Ba/HAP), the highest catalytic performance was achieved between all those catalysts nonthermally treated for the decomposition of $Ba(NO_3)_2$ (#1 to #4 in Table 3). It is worth noticing that the phenomenon of the decrease of the average ammonia production rate when the total pressure was increased to 25 bar was systematically observed.

Finally, in order to improve the catalytic activity of the Ba-containing catalysts, the decomposition of $Ba(NO_3)_2$ was also performed at 600 °C under Ar (see section 2.2). As expected, both the catalyst pretreated under Ar (#5 and #6 in Table 3 for 1Ru2Ba/HAP_Ar and 1Ru1Cs1Ba/HAP_Ar, respectively) shows much higher average ammonia production rates in comparison with their counterparts (#4 and #2 in Table 3 for 1Ru2Ba/HAP

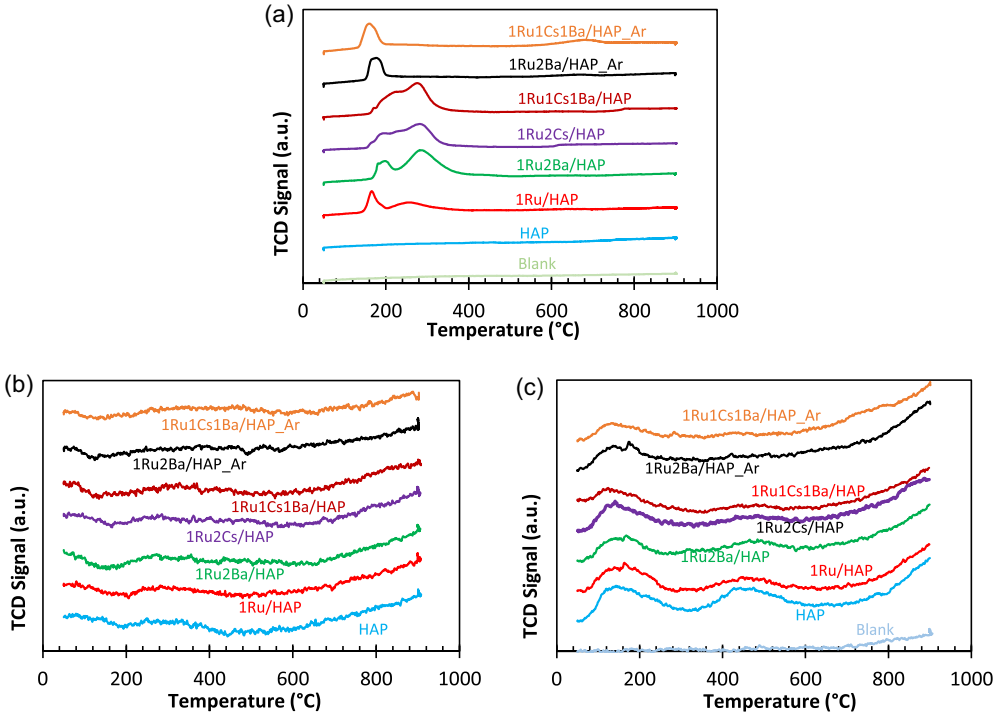

Figure 7. a) TPR, b) CO_2-TPD, and c) NH_3-TPD of the HAP support and the prepared catalyst catalysts; 1Ru/HAP was calcined at 300 °C under air flow, while other multimetallic catalysts were dried at 105 °C.

Table 3. Catalytic performance of the prepared materials in ammonia synthesia.

Entry	Catalyst	Catalyst mass [mg]	Average Production Rate [μmol h^{-1} $g_{cat}{}^{-1}$]					Average N_2 conversion × 10^2 [%]					Average TOF value × 10^4 [s^{-1}]				
#1	1Ru/HAP	297	0	0	0	4	14	0	0	0	0.1	0.2	0	0	0	0.1	0.4
#2	1Ru1Cs1Ba/HAP	301	≈0	24	92	30	70	0	≈0	1	0.7	1.6	0.7	2.5	2.8	0.3	0.2
#3	1Ru2Cs/HAP	317	≈0	17	55	14	48	0	≈0	0.6	0.3	1.1	0	0.5	0.2	0.1	1.4
#4	1Ru2Ba/HAP	303	2	83	265	96	134	0	≈0	0.3	2.1	2.9	0.1	2.3	7.5	2.7	3.8
#5	1Ru2Ba/HAP_Ar	303	88	517	1038	687	975	0.01	5.7	11.4	14.5	20.6	2.5	14.6	29.3	19.4	27.6
#6	1Ru1Cs1Ba/HAP_Ar	306	0	129	323	335	575	0	1.4	3.6	7.2	12.4	0	3.6	9.1	9.5	16.2
Conditions[a)]	Reaction temperature (°C)		350	400	450	450	500	350	400	450	450	500	350	400	450	450	500
	Total reaction pressure (bar)		10	10	10	25	25	10	10	10	25	25	10	10	10	25	25
	Feed volume ratio H_2/N_2		75/50	75/50	75/50	75/25	75/25	75/50	75/50	75/50	75/25	75/25	75/50	75/50	75/50	75/25	75/25
	Reaction step order		1st	2nd	3rd	4th	5th	1st	2nd	3rd	4th	5th	1st	2nd	3rd	4th	5th

[a)]The plateau reaction time was kept for more or less 24 h at each condition of temperature and pressure (see section 2.4). TOF: Turnover frequency.

and 1Ru1Cs1Ba/HAP, respectively). Their TOF values are much higher than those of other catalysts. This is explained through the higher availability of Ba on the surface of the catalysts pretreated under Ar.

Figure 8 compares the cumulative ammonia production over the different investigated catalysts. As expected, the 1Ru2Ba/HAP_Ar catalyst (#5 in Table 3) shows the highest amount of accumulated ammonia produced. However, this catalytic performance is still far from those of the best Ru-based catalysts reported in the literature under similar operation conditions of temperature, pressure, and contact time. For example, Sato et al.[50] obtained the specific ammonia production rate of 90,000 μmol g^{-1} h^{-1} over a Ru/Ba/$LaCeO_x$ at 400 °C, 10 bar and WSHV of 70,000 mL $g_{cat}{}^{-1}$ h^{-1}. A possible reason might be related to the large size of Ru-based nanoparticles in the present work (more or less 20 nm). It is important to reduce the size of Ru nanoparticles on the surface of HAP support by using other synthesis method, such as cation exchange.[51] This may improve the dispersion of Ru, which in turn is expected to improve the catalytic performance of the HAP-supported Ru catalysts. This will be investigated in future work.

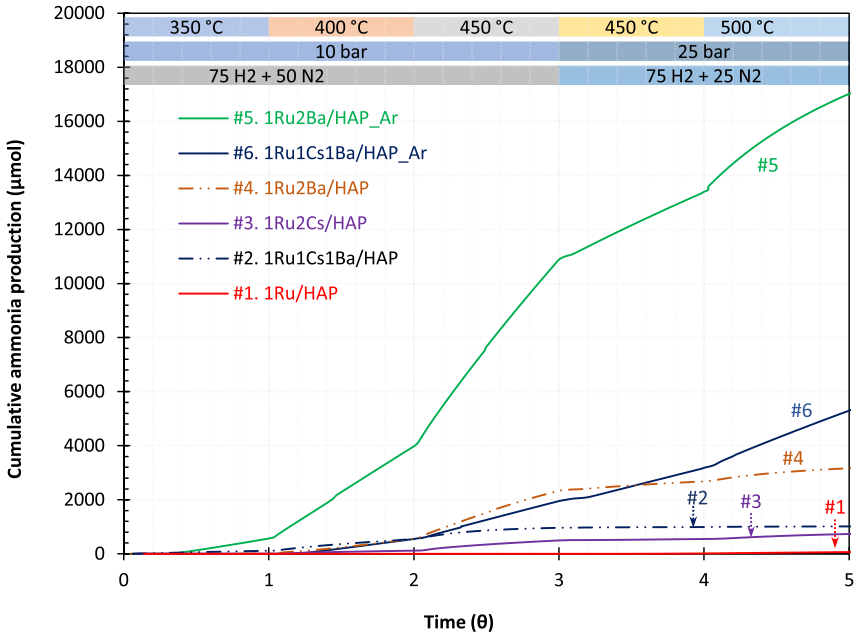

Figure 8. Comparison of the cumulative ammonia production. Θ represents a nondimensional, standardized time such that all experiment stages and the all tests have equal durations.

3. Conclusion

For the first time, HAP-supported Ru catalysts, with and without Ba and/or Cs promotion, have been developed for the ammonia synthesis reaction. By using the conventional incipient wetness impregnation (IWI) method, large Ru, Ba, and Cs nanoparticles were formed on the surface of HAP support. In ammonia synthesis, an unpromoted 1Ru/HAP catalyst showed negligible activity because of the large size of Ru nanoparticles. The addition of Cs and Ba as catalyst promoters enhanced the catalytic activity of the 1Ru/HAP catalyst, and Ba was found to be better than Cs. This could be related to the fact that the addition of Ba and/or Cs decreased the acidity of the HAP-supported Ru catalysts, as highlighted by NH_3-TPD results, which may favor the desorption of NH_3 species formed on the catalyst surface. It is also worth noticing that the decomposition of the Ba precursor ($Ba(NO_3)_2$) needs a specific pretreatment condition (under Ar flow at high temperature of 600 °C). Thus, the catalyst 1Ru2Ba/HAP_Ar pretreated under these conditions showed the highest catalytic activity with the average ammonia production rate reaching 1038 mmol h^{-1} g cat^{-1} at 450 °C and 10 bar with an estimated TOF of 0.0029 s^{-1}. However, this is still far from the performances of other Ru-based catalysts reported in the literature, especially those involving lanthanides under similar conditions.[52]

Further work would focus on the improvement of Ru and Ba deposition on HAP surface by employing other deposition methods, such as cation exchange or deposition-precipitation, hopefully, minimizing particle sizes to single digit nanometers. The resulting catalysts would also be tested at higher pressures, which favor the ammonia synthesis reaction.

4. Experimental Section

Chemicals

A commercial stoichiometric HAP with the theoretical Ca/P molar ratio of 1.67 (information provided by industrial producer) and a surface area (S_{BET}) of 75 m^2 g^{-1} was used as the support material. Ruthenium nitrosyl nitrate (CAS 34513-98-9), barium nitrate (CAS 10022-31-8), and cesium nitrate (CAS 7789-18-6) were purchased from Thermo Scientific to be used as metal precursors.

Catalyst Synthesis

The deposition of the active phases on the HAP support was performed by the standard IWI method, which is the simplest and most widely employed method in catalysis research and the industry.[53] Thus, the wettable volume of HAP was determined. Then, aqueous solutions of the precursors were prepared and used to impregnate adequate amounts of HAP. The mixtures were dried at 105 °C for 24 h and then heated to 300 °C (10 °C min^{-1}) under flowing air and kept at this temperature for 2 h, leading to the formation of the monometallic catalyst (1Ru/HAP). For the preparation of bimetallic catalysts, $Ba(NO_3)_2$ or $CsNO_3$ was deposited on 1Ru/HAP by the IWI method. Then, the mixture was dried at 105 °C for 24 h, and the resulting material is called 1Ru2Ba/HAP or 1Ru2Cs/HAP, respectively. Finally, the trimetallic catalyst (1Ru1Cs1Ba/HAP) was obtained by depositing $Ba(NO_3)_2$ onto 1Ru1Cs/HAP by the IWI method, and then dried at 105 °C for 24 h. Table 2 shows the list of the catalysts prepared in this work, where the order of the appearance of metals indicates the order of their impregnation, while the number indicates the targeted mass percentage of the active metal. As an example, 1Ru1Cs1Ba/HAP means the deposition of 1 wt%Ru, 1 wt%Cs, and 1 wt%Ba at the first, the second, and the third impregnation step, respectively.

In order to facilitate the decomposition of $Ba(NO_3)_2$ into BaO, two Ba-containing catalysts were also pretreated at 600 °C under Ar flow (1Ru2Ba/HAP_Ar and 1Ru1Cs1Ba/HAP_Ar in Table 2).[38] It is also worth noticing that high-temperature treatments (above 700 °C) would preferably be avoided on Cs-containing samples as Cs compounds tend to decompose and volatilize.[39] This is discussed in the results section. Elemental analysis was attempted using the inductively coupled plasma-atomic emission spectroscopy technique, but the complete dissolution of Ru-based nanoparticles was not possible regardless of the concentrated acid mixtures used.

Catalyst Characterization

CHNS analysis was performed on fresh catalysts employing a FLASH 2000 CHNS/O analyzer (Thermo Scientific). This analysis is used to determine the presence of nitrated species on the catalyst samples and to corroborate the decomposition of the metal precursors.

Nitrogen adsorption/desorption isotherms were carried out at 77 K with a Micromeritics TriStar II 3020 and the Micromeritics 3FLEX. Previous outgassing of the samples was performed at 105 °C under vacuum for 48 h. Around 300 mg was employed for each analysis. The Brunauer–Emmet–Teller (BET) model was used to calculate the specific surface area, and the BJH model to determine the mesoporosity of the samples.

TGA was conducted with a DT Q600 apparatus (TA Instruments) under air flow (100 mL min^{-1}), and with a LABSYS evo (Setaram) under Ar flow (100 mL min^{-1}) from 30 °C up to 900 °C at a heating rate of 10 °C min^{-1}. All TG analyses were performed employing Pt crucibles. The dried samples were analyzed by TGA to determine the decomposition temperatures of the metal precursors to form metal oxide nanoparticles. For Ba-containing catalysts, samples were also analyzed under the Ar atmosphere to determine the temperature of decomposition of $Ba(NO_3)_2$ as described by Bardwell et al.[38]

All temperature programmed analyses (TPX) were performed on an AutoChem II/HP from Micromeritics. Masses around 160 mg were employed in all TPX analyses. A flow rate of 50 mL min^{-1} was set for all employed gas mixtures. A cooling trap made from ethylene glycol was prepared to condensate any H_2O and said trap was integrated in all TPX measurements. All heating ramps were set to 5 °C min^{-1}. The TPR analysis starts with a cleaning procedure at 105 °C for 1 h employing an Ar flow, followed by the saturation of the system with 5 vol.% H_2/Ar at 50 °C and the subsequent measurement of its consumption as the temperature rises up to 900 °C. The TPD analysis starts with a TPR procedure to prepare the sample, where the maximum temperature is set to 350 °C and maintained for 2 h. After the sample was saturated with the respective gas mixture, followed by the measurement of the desorption of the probe gas as temperature rises up to 900 °C. Mixtures of 5 vol.% NH_3/He and 5 vol.% CO_2/N_2 are employed in the TPD-NH_3 and TPD-CO_2, respectively. Using ammonia (NH_3-TPD) and carbon dioxide (CO_2-TPD) as probe molecules, the density, and the strength of the acidity and basicity, respectively, can be determined.[54]

SEM coupled with EDX analysis was performed on fresh and used catalyst samples, using a Quattro ESEM (Thermo Fisher Scientific) model S equipped with a field emission gun operating at an acceleration voltage of 6 kV. The samples were dispersed on a double-faced, fixed, adhesive carbon-based support for direct observation of the sample under low vacuum (0.48 mbar). The mode of operation was backscattered electron.

TEM coupled with EDX analysis was performed on fresh samples, using a JEM-2100F Field Emission Electron Microscope (JEOL) operating at a potential difference of 200 kV. Similarly, scanning transmission electron microscopy analysis was performed at 200 kV. All images were captured employing a CMOS Rio 16IS camera (Gatan). EDX analysis was performed using an 80 m2 EDX UltimMax (Oxford Instruments).

XRD analysis was performed on fresh catalysts using a Malvern PANalytical Empyrean X-Ray Powder Diffractometer operating in reflection (Bragg–Brentano geometry) and θ–θ mode. X-rays are generated by a tubular anticathode of Cu Kα radiation ($\lambda = 0.15418$ nm) and measured by 1Der detector. Data were collected by operating at 45 kV, 40 mA within the angular range 2θ from 7° to 80° with a measurement step size of 0.0167° (2θ) at a rate of 160 s/step.

FTIR spectra of the fresh catalysts were recorded with a Thermo Scientific NicoletTM iS10 FTIR spectrometer employing the Smart iTX ATR (Attenuated Total Reflectance) attachment equipped with a Ge crystal. The OMNICTM software package was employed for data retrieval. Samples were studied at mid-IR, i.e., from 4000 to 500 1/cm (650 cm^{-1} for some samples), with 64 averaged measurements.

Catalytic Experiments

The reaction of ammonia synthesis was performed using a fixed-bed reactor. For each experiment, the reactor was loaded with ca. 300 mg of powder catalyst, which was diluted twice with an alumina powder sintered at 1000 °C for 5 h (specific surface area smaller than 3 $m^2 g^{-1}$). For this loading step, the reactor tube was first filled with around 4 g of the sintered alumina powder, followed by the catalyst which was located at the center of the reactor tube, and finally around 6 g of the sintered alumina powder. After an in situ reduction at 350 °C (10 °C min^{-1}) for 2 hr under pure H_2 (100 mL min^{-1}), the reactor was fed with a mixture of H_2 (75 mL) and N_2 (50 mL) to start the ammonia synthesis reaction at 350 °C reaction temperature and 10 bar total reaction pressure. The gas mixture at the reactor outlet was analyzed by an inline μ-GC. For each catalyst, details on the conditions of reaction temperature and pressure are as follows:

1) The first reaction step: The reaction was kept at 350 °C, and the total pressure was raised to 10 bar (from atmospheric), the flow of H_2 (75 mL) and N_2 (50 mL) are set and these conditions were maintained for 22 h. 2) The second reaction step: The temperature was increased to 400 °C (10 °C min^{-1}), the other conditions remained unchanged and were kept for 22 h. 3) The third reaction step: The temperature was increased to 450 °C (10 °C min^{-1}), the other conditions remained unchanged and were kept for 22 h. 4) The fourth reaction step: The temperature was maintained at 450 °C, the flow of H_2 (75 mL) and N_2 (25 mL) was altered, the total pressure was raised to 25 bars and this operation regime was kept for 16 h. 5) The fifth reaction step: The temperature was increased to 500 °C (10 °C min^{-1}), the other conditions remain unchanged and unaltered for 16 h.

The inlet molar ratio of H_2 to N_2 was kept at 3/2, which is smaller than the stoichiometry of ammonia synthesis. This is because previous works have identified that inlet mixtures rich in H_2 to poison Ru-based catalysts.[28]

Acknowledgements

This work was cofunded by the Occitanie region (France) via the *Pôle RHyO*, IMT Mines Albi, and the enterprise Khimod in the framework of the Ph.D. project named SYNTAC, which is gratefully acknowledged. This Ph.D. project was also labeled by EUR BIOECO in the framework of the "*Investissements d'Avenir*" program (ANR-18-EURE-0021).

Conflict of Interest

The authors declare no conflict of interest.

Data Availability Statement

The data that support the findings of this study are available from the corresponding author upon reasonable request.

Keywords: ammonia synthesis · barium · catalysis · hydroxyapatite · ruthenium

[1] M. Appl, *Ammonia: Principles and Industrial Practice*, Wiley-VCH, Weinheim **2021**.
[2] L. Wang, M. Xia, H. Wang, K. Huang, C. Qian, C. T. Maravelias, G. A. Ozin, *Joule* **2018**, *2*, 1055.
[3] J. Li, Q. Xiong, X. Mu, L. Li, *ChemSusChem* **2024**, *17*, e202301775.
[4] E. Castillejos, E. García-Bordejé, *ChemCatChem* **2024**, *16*, e202301603.
[5] K. E. Lamb, M. D. Dolan, D. F. Kennedy, *Int. J. Hydrogen Energy* **2019**, *44*, 3580.
[6] E. W. Lemmon, I. H. Bell, M. L. Huber, M. O. McLinden, **2018**, https://doi.org/10.18434/T4/1502528.
[7] International Energy Agency, *Ammonia Technology Roadmap: Towards More Sustainable Nitrogen Fertiliser Production*, OECD **2021**.
[8] M. Aziz, F. B. Juangsa, A. R. Irhamna, A. R. Irsyad, H. Hariana, A. Darmawan, *J. Energy Inst.* **2023**, *111*, 101365.
[9] G. Ertl, D. Prigge, R. Schloegl, M. Weiss, *J. Catal.* **1983**, *79*, 359.
[10] A. Casalot, A. Durupthy, *Chimie Inorganique: Cours, 2e Cycle*, Hachette, Paris **1993**.
[11] J. M. Thomas, W. J. Thomas, *Principles and Practice of Heterogeneous Catalysis*, John Wiley & Sons, Weinheim **2015**.
[12] Heraeus, *K-04502 | Ruthenium | Spheres*, https://www.heraeus-precious-metals.com/en/products-solutions-by-category/heterogeneous-catalysts/catalyst-selector/cc-ps-detail/5119272/ (accessed 19 March 2025) n.d.
[13] J. C. Verschoor, P. E. de Jongh, P. Ngene, *Curr. Opin. Green Sustainable Chem.* **2024**, *50*, 100965.
[14] J. Humphreys, R. Lan, S. Tao, *Adv. Energy Sustainability Res.* **2021**, *2*, 2000043.
[15] K. Honkala, A. Hellman, I. N. Remediakis, A. Logadottir, A. Carlsson, S. Dahl, C. H. Christensen, J. K. Nørskov, *Science* **2005**, *307*, 555.
[16] S. R. Tennison, in *Catalytic Ammonia Synthesis: Fundamentals and Practice* (Ed: J. R. Jennings) Springer US, Boston, MA, **1991**, pp. 303–364.
[17] I. Rossetti, N. Pernicone, L. Forni, *Appl. Catal., A* **2001**, *208*, 271.
[18] I. Rossetti, F. Mangiarini, L. Forni, *Appl. Catal., A* **2007**, *323*, 219.
[19] X. Ju, J. Feng, J. Wang, J. Guo, L. Liu, *Catal. Lett.* **2022**, *153*, 1615.
[20] Y. V. Larichev, *J. Phys. Chem. C.* **2011**, *115*, 631.
[21] T. Hughes, F. Liao, S. C. Tsang, I. Wilkinson, S. S. S. Wu, *Catalyst for Ammonia Synthesis*, **2018**, WO/2018/215202.
[22] V. A. Borisov, P. A. Fedotova, K. N. Iost, V. L. Temerev, Y. Surovikin, A. B. Arbuzov, M. Trenikhin, D. A. Shlyapin , in *Oil and Gas Engineering (Oge-2020)* (Eds: A. V. Myshlyavtsev, V. A. Likholobov, V. L.Yusha), American Institute of Physics, Melville **2020**, p. 020004.
[23] V. A. Borisov, K. N. Iost, V. L. Temerev, P. A. Fedotova, Y. V. Surovikin, A. B. Arbuzov, M. V. Trenikhin, D. A. Shlyapin, *Diamond Relat. Mater.* **2020**, *108*, 107986.
[24] K. N. Iost, N. S. Smirnova, V. A. Borisov, V. L. Temerev, Y. V. Surovikin, V. V. Kriventsov, E. V. Khramov, Y. V. Zubavichus, M. V. Trenikhin, E. Y. Gerasimov, D. A. Shlyapin, P. G. Tsyrul'nikov, *Russ. J. Phys. Chem.* **2020**, *94*, 2201.
[25] K. N. Iost, V. A. Borisov, V. L. Temerev, Y. V. Surovikin, P. E. Pavluchenko, M. V. Trenikhin, A. A. Lupanova, A. B. Arbuzov, D. A. Shlyapin, P. G. Tsyrulnikov, A. A. Vedyagin, *Surf. Interfaces* **2018**, *12*, 95.
[26] B. Lin, K. Wei, J. Ni, J. Lin, *ChemCatChem* **2013**, *5*, 1941.
[27] J. Ni, J. Lin, X. Wang, B. Lin, J. Lin, L. Jiang, *ChemistrySelect* **2017**, *2*, 6040.
[28] I. Rossetti, N. Pernicone, F. Ferrero, L. Forni, *Ind. Eng. Chem. Res.* **2006**, *45*, 4150.
[29] I. Rossetti, N. Pernicone, L. Forni, *Catal. Today* **2005**, *102-103*, 219.
[30] N. B. Shitova, N. M. Dobrynkin, A. S. Noskov, I. P. Prosvirin, V. I. Bukhtiyarov, D. I. Kochubei, P. G. Tsyrul'nikov, D. A. Shlyapin, *Kinet. Catal.* **2004**, *45*, 414.
[31] N. S. Smirnova, V. A. Borisov, K. N. Iost, V. L. Temerev, J. V. Surovikin, T. I. Guljaeva, A. B. Arbuzov, P. G. Cyrul'nikov, *Procedia Eng.* **2015**, *113*, 84.
[32] Y. Ma, G. Lan, W. Fu, Y. Lai, W. Han, H. Tang, H. Liu, Y. Li, *J. Energy Chem.* **2020**, *41*, 79.
[33] B. Lin, Y. Guo, C. Cao, J. Ni, J. Lin, L. Jiang, *Catal. Today* **2018**, *316*, 230.
[34] F. R. García-García, A. Guerrero-Ruiz, I. Rodríguez-Ramos, *Top. Catal.* **2009**, *52*, 758.
[35] X. Li, X. Zhang, H. O. Everitt, J. Liu, *Nano Lett.* **2019**, *19*, 1706.
[36] D. P. Minh, *Design and Applications of Hydroxyapatite-Based Catalysts*, WILEY-VCH, Weinheim **2022**.
[37] D. Uner, M. Y. Aslan, S. Akbayrak, S. Özkar, *Social Science Research Network*, https://papers.ssrn.com/sol3/papers.cfm?abstract_id=4709925 (accessed: September 2025).
[38] C. J. Bardwell, R. I. Bickley, S. Poulston, M. V. Twigg, *Thermochim. Acta* **2015**, *613*, 94.
[39] P. F. Campbell, M. H. Ortner, C. J. Anderson, *Anal. Chem.* **1961**, *33*, 58.
[40] A. Prihanto, S. Muryanto, R. Ismail, J. Jamari, A. P. Bayuseno, *Inorg. Chem. Commun.* **2023**, *157*, 111301.
[41] M. Janek, I. Vašková, M. Pischová, R. Fialka, Z. Hajdúchová, P. Veteška, J. Feranc, M. H.áth Orlovská, P. Peciar, E. Rakovský, Ľ. Bača, *J. Eur. Ceram. Soc.* **2024**, *44*, 5284.
[42] M. E. Fleet, X. Liu, *Biomaterials* **2005**, *26*, 7548.
[43] Y. Guo, Y. Zhou, D. Jia, H. Tang, *Microporous Mesoporous Mater.* **2009**, *118*, 480.
[44] S. Brunauer, L. S. Deming, W. E. Deming, E. Teller, *J. Am. Chem. Soc.* **1940**, *62*, 1723.
[45] S. M. Ghoreishian, K. Shariati, Y. S. Huh, J. Lauterbach, *Chem. Eng. J.* **2023**, *467*, 143533.
[46] H.-Y. Chen, S.-Y. Chen, Y. I. A. Reyes, M. Keller, T. Mochizuki, C.-N. Liao, H.-Y. T. Chen, *EnergyChem* **2024**, *6*, 100140.
[47] Y. Wang, Y. Jiang, Y. Yuan, L. Xu, W. Sun, S. Wu, Q. Wang, N. Hu, L. Wang, *J. Alloys Compd.* **2025**, *1010*, 177610.
[48] G. Lin, W. Lin, J. Wu, Y. Zhan, F. Okejiri, M. Weng, J. Fu, *Chem. Eng. Sci.* **2022**, *249*, 117343.
[49] D. Saha, S. Deng, *J. Chem. Eng. Data* **2010**, *55*, 5587.
[50] K. Sato, S. Miyahara, Y. Ogura, K. Tsujimaru, Y. Wada, T. Toriyama, T. Yamamoto, S. Matsumura, K. Nagaoka, *ACS Sustainable Chem. Eng.* **2020**, *8*, 2726.
[51] K. Yamaguchi, K. Mori, T. Mizugaki, K. Ebitani, K. Kaneda, *J. Am. Chem. Soc.* **2000**, *122*, 7144.
[52] M. Kitano, Y. Inoue, M. Sasase, K. Kishida, Y. Kobayashi, K. Nishiyama, T. Tada, S. Kawamura, T. Yokoyama, M. Hara, H. Hosono, *Angew. Chem., Int. Ed.* **2018**, *57*, 2648.
[53] B. A. T. Mehrabadi, S. Eskandari, U. Khan, R. D. White, J. R. Regalbuto, in *Advances in Catalysis* (Ed:C. Song), Academic Press **2017**, pp. 1–35.
[54] M. Miyauchi, T. Watanabe, D. Hoshi, T. Ohba, *Dalton Trans.* **2019**, *48*, 17507.